ORIGINAL ARTICLE

Flexural performance of precast hollow-core slabs strengthened with textile-reinforced highly ductile concrete (TRHDC)

Shifei Song[1] · Mingke Deng[1] · Jiasheng Yang[1] · Ruizhe Li[1] · Yangxi Zhang[1]

Abstract

Textile-reinforced highly ductile concrete (TRHDC) was a promising composite material, which exhibited multiple crack characteristics, high cracking and ultimate tensile strength under uniaxial tension. In this study, six precast hollow-core slabs including one reference slab and five TRHDC-strengthened slabs were manufactured and tested as simply supported under four-point bending. The parameters under investigation included: (i) the TRHDC matrix added with or without polyvinyl alcohol (PVA) fibers, and (ii) the number of textile layers. The test results indicated that adding PVA fibers in the TRHDC matrix could effectively limit the crack width of TRHDC composites, and multi-crack behavior was observed in the strengthening overlay. Besides, TRHDC composites were efficient in enhancing the flexural capacity of strengthened slabs, which were 70–113% in cracking load, and 74–132% in peak load compared with the reference slab. Finally, based on the plane section assumption, an analytical model was given to predict the flexural capacity of TRHDC-strengthened slabs.

Keywords Precast hollow-core slabs · Strengthening · Textile-reinforced highly ductile concrete (TRHDC) · Short polyvinyl alcohol (PVA) fibers · Flexural behavior

1 Introduction

Precast hollow-core slabs had been widely used in low-rise buildings as the advantages of shorten construction period and suitability for industrial production. For many reasons, such as (i) aging of materials, (ii) corrosion of steels due to the large crack opening in concrete, or (iii) increasing load demands due to either change of use or structural interventions, there was a necessity to repair and strengthen the precast hollow-core slabs.

✉ Yangxi Zhang
    yangxizhang@xauat.edu.cn

    Shifei Song
    1169926962@qq.com

    Mingke Deng
    dengmingke@126.com

    Jiasheng Yang
    yangjs178@163.com

    Ruizhe Li
    2353350553@qq.com

1   School of Civil Engineering, Xi'an University
    of Architecture and Technology, No. 13, Yanta Road,
    Xi'an 710055, Shaanxi Province, China

Currently, numerous techniques including reinforced concrete (RC) jacketing, externally bonding steel plates, fiber-reinforced polymer (FRP), and so on, were used in the field of strengthening RC members with their pros and cons. In particular, a major disadvantage of RC jacketing was the large strengthening layers of concrete, which the thickness was about 60–70 mm [1–3]. It would greatly limit the usage space of buildings. The externally bonding steel plates were related to their poor fire resistance [4]. As for FRP, the experimental programs [5–10] have demonstrated the outstanding mechanical properties of FRP composites in terms of high strength-to-weight ratio, corrosion, and fire resistance. However, some drawbacks of epoxy adhesive, such as poor fire resistance, low impact resistance, and incompatibility with the wet substrate, have limited the use of FRP.

To amend the problems mentioned above, a highly ductile concrete (HDC) strengthening technique was developed by some scholars. HDC was a typical fiber-reinforced cementitious composite, which exhibited high cracking strength, excellent strain-hardening, and multiple cracking behaviors, also known as engineered cementitious composites (ECC) [11–13]. Hemmati et al. [14, 15] used ECC layers to strengthen the RC beams and slabs. The results illustrated that the application of ECC overlay, as a retrofitting material,

was an efficient procedure to improve the cracking load and limit the crack width. The cracking load was increased by 1.5–2.0 times and the average crack width was about 60 μm after being strengthened by the ECC layer. However, the ultimate load of ECC-strengthened specimens was improved slightly as ECC owned a low ultimate tensile strength with an average value of about 4 MPa [16].

To optimize the mechanical property of HDC, various textiles, such as aramid [17], basalt [18], carbon [19], glass [20], and Polyp-phenylene benzothiazole (PBO) [21], were configured in HDC. It was pre-named as textile-reinforced highly ductile concrete (TRHDC). In terms of characteristics of high tensile strength and large elastic modulus for carbon textile, Dong et al. [22] study the tensile behavior of carbon TRHDC and found that its ultimate tensile strength could reach 12 MPa, which was much greater than the other type of textiles. Barhum et al. [23] indicated that the addition of short fibers could enhance the bond behavior between the textile and HDC by increasing the number of cross-links, which led to the attachment of more hydration products and friction bonds and thereby further improving the tensile strength of TRHDC. Overall, by the combination of carbon textile and HDC, TRHDC exhibited multiple crack characteristics, high cracking and ultimate strength under tension. This composite material showed excellent durability in the harsh environment, regardless of low temperatures or chlorine erosion.

This study investigated the flexural behaviors of precast hollow-core slabs strengthened with TRHDC composites. Six precast hollow-core slabs, including one reference slab and five strengthened slabs, were designed and tested. The test variables were (i) the HDC matrix added with or without PVA fibers, and (ii) the number of textile layers. The failure modes, load–deflection curves, serviceability limit state, energy absorption, and strain analysis were discussed. Finally, based on the plane section assumption, an analytical model was given to predict the flexural capacity of TRHDC-strengthened slabs.

2 Experimental program

2.1 Specimen design

A total of six precast hollow-core slabs were designed, cast, and tested as simply supported under four-point bending. All initial slabs owned the same section dimensions and longitudinal steel bar arrangement, as shown in Fig. 1a. After curing the initial slabs for 28 days, different configurations of TRHDC composites were applied on the tensile side of the slabs to achieve the strengthening, as shown in Fig. 1b. The TRHDC configuration could be illustrated clearly according to Table 1. The first specimen RS was designed as the reference slab. The second specimen SN-C1 was strengthened by TRHDC composites equipped with one layer of carbon textile, while no PVA fibers were added to the matrix. The purpose of adding with or without PVA fibers was mainly to investigate the effect of PVA fiber on the crack width of precast hollow-core slabs. The third specimen SY-C0 was only strengthened by HDC. No textile was applied in the strengthening overlay. The remaining specimens SY-C1,
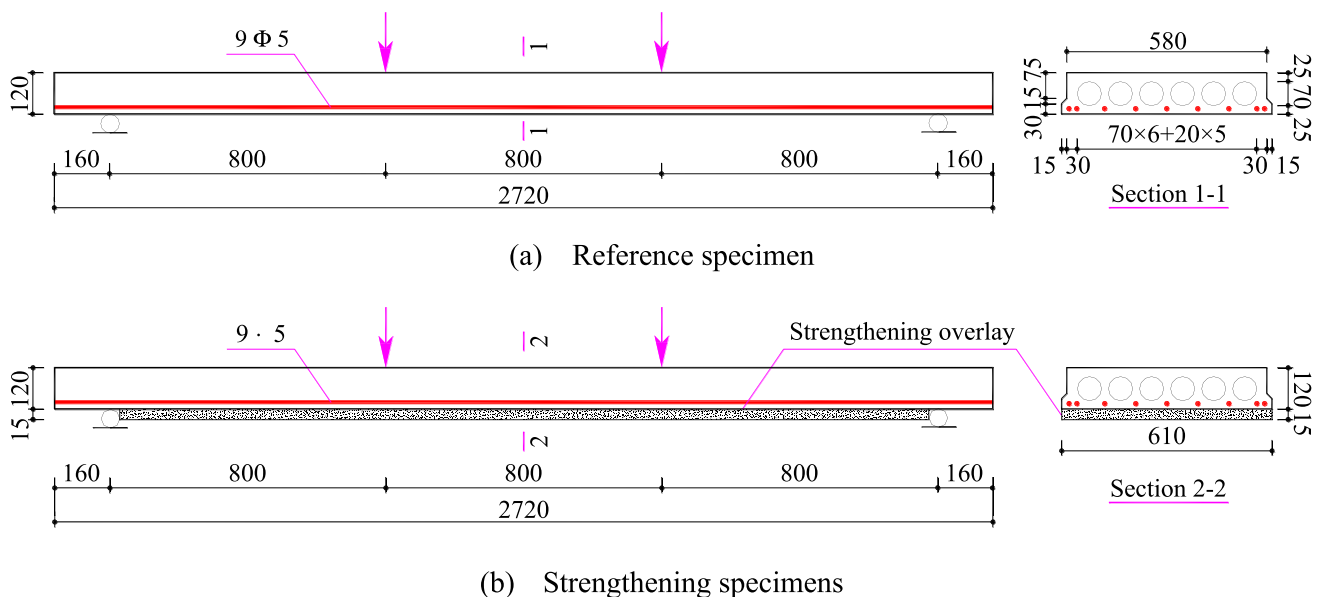

(a)   Reference specimen

(b)   Strengthening specimens

Fig. 1 Specimens details (mm)

Table 1 Main parameters of precast hollow-core slabs

Specimen	Longitudinal steel bar	Type of textile	Layer of textile	Textile reinforcement ratio (%)	PVA content (%)
RS	9 φ 5	–	–	–	–
SN-C1	9 φ 5	Carbon textile	1	0.30	–
SY-C0	9 φ 5	Carbon textile	0	0.00	1.5
SY-C1	9 φ 5	Carbon textile	1	0.30	1.5
SY-C2	9 φ 5	Carbon textile	2	0.60	1.5
SY-C3	9 φ 5	Carbon textile	3	0.89	1.5

SY-C2, and SY-C3 were strengthened by TRHDC composites equipped with one, two, and three layers of carbon textile, respectively.

In Table 1, the notations of specimens were paraphrased as follows. The RS of the first specimen represented the reference slab. In the remaining specimens, the first two characters of the notation "SN" or "SY" mean the HDC matrix added with or without PVA fibers. The third character "C" stood for the type of textile. And the last numbers of "0", "1", "2", and "3" indicated the layers of carbon textile. For example, the SY-C3 represented the specimen strengthened with three layers of carbon textile, and short PVA fibers were added to the HDC matrix.

2.2 Specimens preparation

The initial slabs were designed according to Ref. [24], which was the guideline for precast hollow-core slabs. Before being strengthened by TRHDC, the loose cement layer on the bottom surface of specimens should be removed to ensure a good bonding property at the interface. Subsequently, the specimens needed to be cleaned with water and left in the laboratory for one day to dry out. After the application of the first HDC overlay on the concrete surface, the first layer of carbon textile was attached and pressed slightly into the HDC overlay. The next HDC overlay covered the carbon textile completely, and the operation was repeated until all textiles were applied and covered by HDC. It should be noted that the first and last overlay of HDC was more than 3 mm, and the HDC overlay between textiles was about 2–3 mm. The total thickness of the strengthening layer was 15 mm.

2.3 Material properties

2.3.1 Concrete and longitudinal steel bars

Grade C40 ready-mix normal-weight concrete supplied by a local manufacturer was used to cast the precast hollow-core slabs. The cube compressive strength and uniaxial compressive strength of concrete were 50.10 MPa and 36.00 MPa, respectively. It was tested by three cube samples

(100 mm × 100 mm × 100 mm) and three prism samples (100 mm × 100 mm × 300 mm) according to code GB50010-2010 [25]. The samples were cured under the same conditions as the precast hollow-core slabs.

The longitudinal steel bars of the initial slabs were composed of nine cold-drawn low-carbon steel bars with a diameter of 5 mm (0.2 in.), which were denoted as 9 φ 5 according to the Chinese code [25]. The surface property of the steel bars was plain. The tensile properties of the steel bars were determined by three samples with a length of 30 cm [26]. The typical tensile stress–strain curve was shown in Fig. 2. It could be observed that the stress–strain curve owned no yield platform, which was different from the commonly used hot-rolled ribbed steel bar. Based on the data in Fig. 2, the ultimate tensile strength of the steel bars was 560 MPa.

2.3.2 TRHDC composites

TRHDC composites consisted of carbon textiles and HDC. The carbon textile was woven from carbon fibers and coated with epoxy on the surface to fix the shape. In the uniaxial tensile tests, the carbon textile exhibited linear elastic
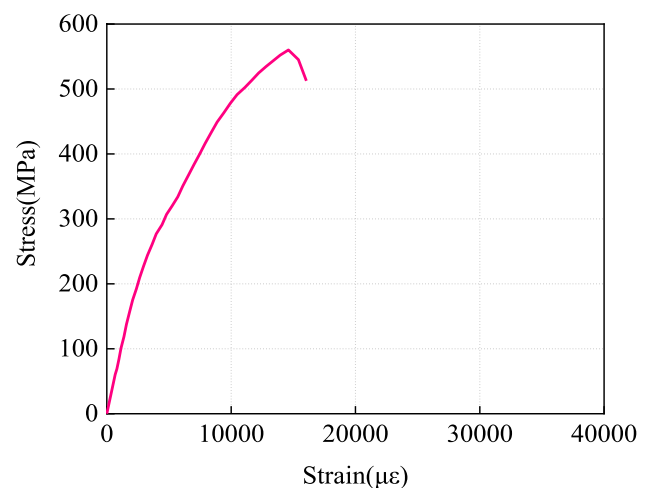

Fig. 2 Tensile stress–strain curve of longitudinal steel bar

behaviors up to brittle rupture failure. The test results were shown in Table 2 based on code GB/T 36262–2018 [27].

HDC was composed of water, silica sand, and cementing material (42.5R Portland cement and fly ash) in a homologous ratio of 0.29: 0.36:1. The cube compressive strength of HDC without adding PVA fibers was 55.44 MPa. Considering the mix workability and fiber dispersion, 1.5% volume content of PVA fiber was added in the HDC to improve the cracking strength and limit the crack width. The mechanical properties of PVA fibers were shown in Table 3.

The cube compressive strength of HDC added with PVA fibers was 60.40 MPa, which was higher than the above one without PVA fibers. The reason was the bridging effect of PVA fibers limited the development of cracks, increasing the compressive strength. The tensile properties of HDC and TRHDC were measured by dog-bone-shaped samples [28], as shown in Fig. 3a. The typical tensile stress–strain curves were shown in Fig. 3b. The main test results were listed in Table 4.

The workability of the fresh HDC was assessed by slump flow tests, and the measured slump flow diameter of the fresh HDC was shown in Fig. 4. The average slump flow diameter of the fresh HDC before and after the addition of PVA fibers was 620 mm and 190 mm, respectively. It could be concluded that the addition of PVA fiber weakened the workability of HDC. However, the weakened workability of HDC made it very easy to be trowelled to the bottom surface of the slabs in practical projects.

2.4 Test setup

The specimens were tested under four-point flexural loading with a clear span of 2400 mm. The length of the constant moment zone was 800 mm. The test was carried out by a 1000 kN-capacity servo-hydraulic actuator at a rate of 0.2 mm/min, as shown in Fig. 5. Two linear variable differential transformers (LVDTs) were employed on the tensile side to measure the mid-span deflection. Five strain gauges with a base length of 100 mm were arranged along the specimen height to measure the strain of the concrete. Besides, another concrete strain gauge was set in the strengthening overlay to observe the slippage between the TRHDC overlay and concrete substrate. The specific positions of the strain gauge were shown in Fig. 6. During

the test, the occurrence and development of cracks should also be recorded in real-time.

3 Experimental results and discussions

3.1 Failures modes and cracks distribution

The typical failure modes (Fig. 7a) and crack distribution (Fig. 7b–g) in the tensile side of specimens were presented in Fig. 7.

3.1.1 Reference specimen RS

As can be seen in Fig. 7b, the flexural crack initiated in the tensile side of the constant moment zone, and they spread gradually to the top side of the specimen. Finally, the reference specimen RS failed in flexure after the formation of large flexural cracks. The failure was due to the fracture of longitudinal steel bars. At this moment, the concrete at the edge of the compression zone was not crushed.

3.1.2 Strengthened specimen

The specimen SN-C1 was strengthened by TRHDC composites equipped with one layer of carbon textile. No PVA fibers were added to the HDC matrix. The specimen failed in the flexural failure mode characterized by textile rupture. Meanwhile, the longitudinal steel bars were not fractured, and the concrete at the edge of the compression zone was not crushed. The final crack distribution was shown in Fig. 7(d). As for specimens SY-C0, SY-C1, SY-C2, and SY-C3, which added PVA fibers into the HDC matrix, the crack distribution was very different from that of SN-C1. The first vertical crack was found at the interface between the original slab and the strengthening layer. Subsequently, the cracks passed through the strengthening layer and transformed into two or more finer secondary cracks. The reason was the PVA fibers across the cracks could still transmit the tensile force (bridging effect), which was different from the tensile properties of normal concrete. The failure mode of these four specimens was similar to specimen SN-C1, where the rupture of the strengthening overlay was observed at the large crack.

Compared with specimen SN-C1, the crack numbers were increased. While the crack width was reduced obviously. Multi-crack behavior was observed in the strengthening

Table 2 Geometrical and mechanical properties of carbon textile

Nominal spacing (mm)	Young's modulus (GPa)	Tensile strength (MPa)	Strain (%)	Density (g/cm³)
20×20	239	3600	1.45	1.74

Table 3 Mechanical properties of PVA fiber

Length (mm)	Diameter (μm)	Tensile strength (MPa)	Tensile modulus (GPa)	Elongation (%)	Specific gravity (g/cm²)
12	39	1600	32	7	1.29

(a) Dog-bone-shaped samples   (b) Tensile stress-strain curves of HDC and TRHDC composites
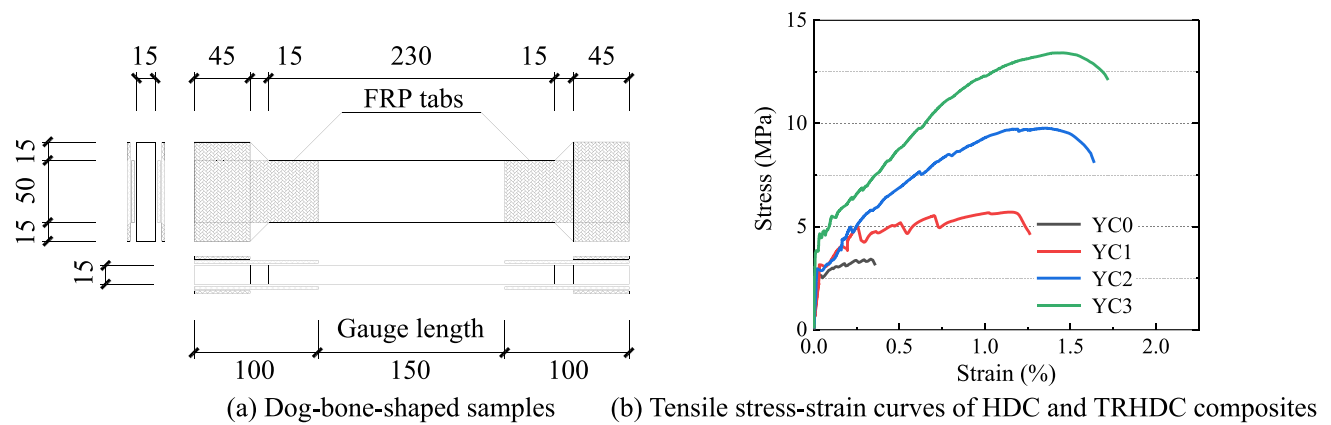
Fig. 3 Parameters associated with the dog-bone-shaped samples

Table 4 Mechanical properties of concrete, HDC, and TRHDC composites

Samples	Corresponding slab	Cracking strain (%)	Cracking strength (MPa)	Peak strain (%)	Peak strength (MPa)
Concrete	–	0.019	2.01	0.019	2.01
YC0	SY-C0	0.025	2.98	0.70	3.42
NC1	SN-C1	0.021	3.61	0.80	5.16
YC1	SY-C1	0.025	4.37	0.75	6.43
YC2	SY-C2	0.027	4.94	0.85	9.34
YC3	SY-C3	0.032	5.01	1.10	11.42

Note: YC0, YC1, YC2, and YC3 represented the dog-bone-shaped samples configured with 0, 1, 2, and 3 layers of textiles, respectively. Besides, the PVA fibers were added to HDC. NC1 represented the dog-bone-shaped sample configured with 1 layer of textile, and no fiber was added to HDC

layer due to the bridging effect of PVA fibers. It could also be observed that the textile ruptured around the large crack, and then pulled out at this crack. And the yarns of textiles were ruptured from the outer filament ring to the core filaments gradually, as reported in Ref. [7].

3.2 Load–deflection response

The load–deflection curves of all test specimens were depicted in Fig. 8. Combined with Fig. 8 and field records, the test results of characteristic points were summarized in Table 5, including the cracking load (F_{cr}), peak load (F_p), ultimate load (F_u), and correspondent deflection (Δ_{cr}, Δ_P, and Δ_u, respectively).

It could be observed that the curves were roughly composed of three phases, which were (i) the linear segment before cracking, (ii) the stiffness reduction segment after cracking to failure, and (iii) the post-failure segment. In the first segment, the curves of all specimens coincided roughly, indicating that there was no obvious difference in the elastic stiffness between the strengthened specimens and the reference one. After cracking, the specimens exhibited a

reduction in stiffness due to the appearance of cracks. While for the strengthened specimen, the deflection was less than the reference specimen at the equivalent load level, and the deflection was reduced further as the number of textile layers increased. It indicated that the TRHDC composites were favorable for improving the stiffness of specimens. This can be explained by the fact that more textiles could afford more tensile force, and the effect of textiles in limiting the development of cracks was also increased, which delayed the stiffness degradation of specimens. As a result, the specimen rigidity was enhanced, and the deflection was suppressed. After the peak point, the load–deflection curves began to decline due to the fracture of longitudinal steel bars (for reference specimen RS), the rupture of textiles (for strengthened specimens SN-C1, SY-C1, SY-C2, and SY-C3), and the slow pulling-off or pulling-out of PVA fiber (for strengthened specimen SY-C0).

The obvious effect of strengthening was noticed at cracking load. Compared with the reference specimen RS, the cracking load of SN-C1 only increased by 28%. The cracking load could hardly be improved by TRHDC composites without adding PVA fibers, even if one layer of carbon
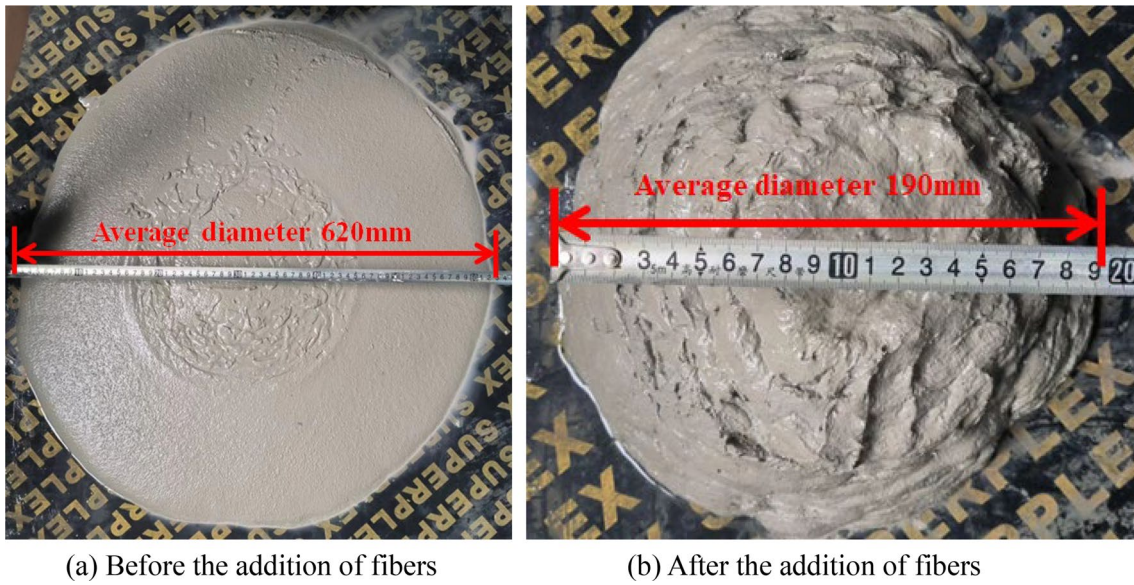
(a) Before the addition of fibers   (b) After the addition of fibers

Fig. 4 Diagram of the slump flow test results

Fig. 5 Test setup

textile was embedded in the matrix. The reason was the ultimate tensile strain of carbon textiles was 1.45%, which was far greater than the cracking strain of the matrix. The tensile stress of the carbon textiles was at a low level before cracking. For specimen SY-C1 which added PVA fibers in matrix,

the cracking load was increased by 70%. It was higher than the value of SN-C1. The reason was the bridging effect of PVA fibers limited the development of cracks, which was effective to improve the cracking load. It could also be noticed that the peak load of SY-C1 was higher than SN-C1 slightly. In addition to the fact that the PVA fibers across the cracks could continue to transfer tensile force, another major reason was the PVA fibers improved the utilization of carbon textiles (Explained by cross-link theory in Ref. [23]).

As can be seen in Table 5, the peak load of strengthened specimens SY-C0, SY-C1, SY-C2, and SY-C3 was 22.19kN, 31.70kN, 39.96kN, and 42.26kN. Compared with the reference specimen RS, the peak load was increased by 22%, 74%, 119%, and 132%, respectively. More textiles were beneficial for improving the peak load, while the increment in peak load was non-proportional to the number of textiles layers. This was related to the bonding property between the textile and the matrix. The carbon textiles were woven
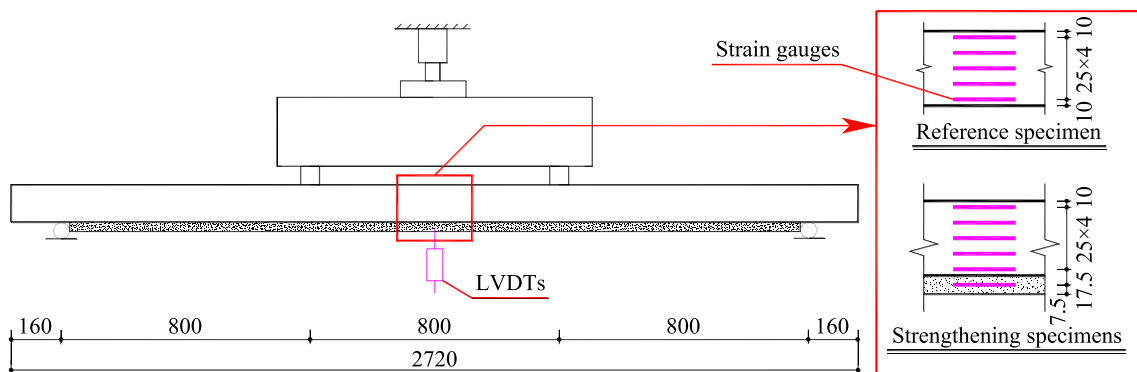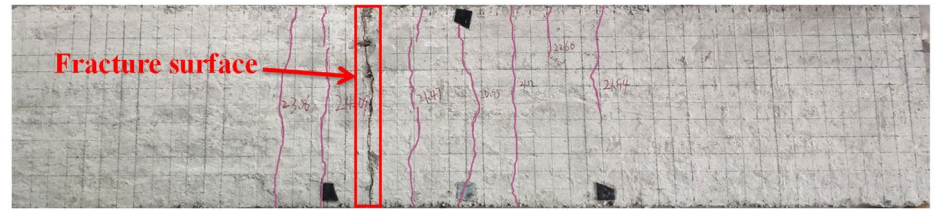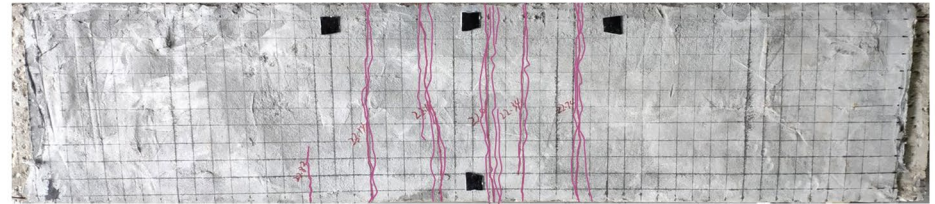

Fig. 6 Measuring point setup

Fig. 7 Failure modes and cracks distribution
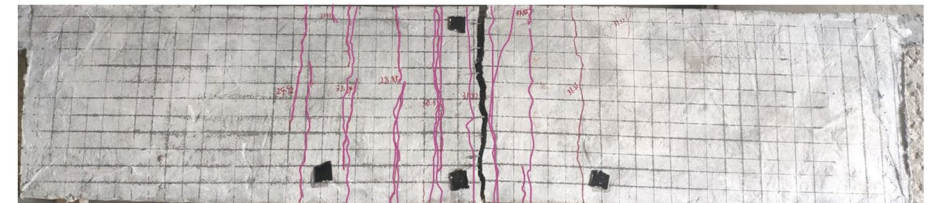
(a) Typical failure mode

Fracture surface →

(b) RS

(c) SY-C0

(d) SN-C1

(e) SY-C1

(f) SY-C2

(g) SY-C3

(a) Effect of HDC matrix added with or
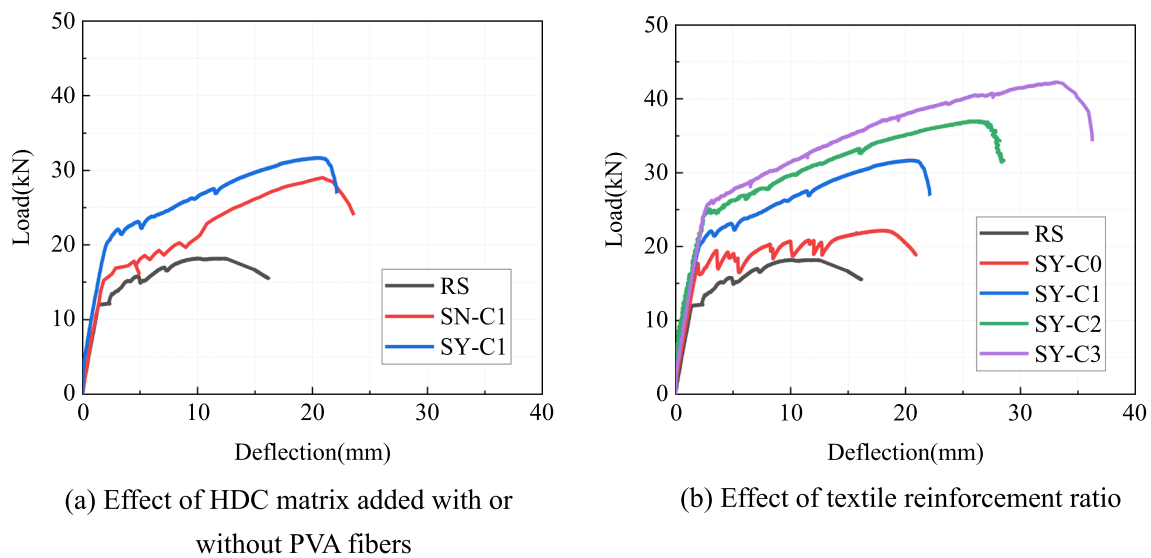without PVA fibers

(b) Effect of textile reinforcement ratio
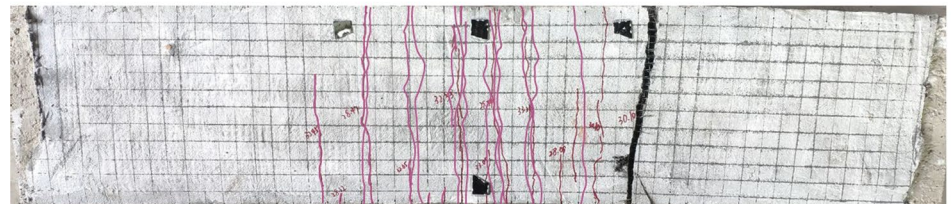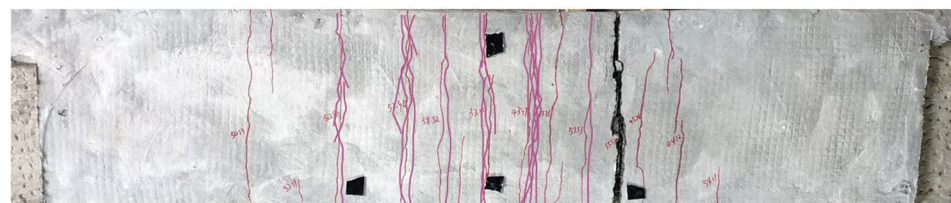
Fig. 8 Load–deflection curves

Table 5 Test results

Specimen	F_{cr} (kN)	Increase in F_{cr} (%)	Δ_{cr} (mm)	F_p (kN)	Increase in F_p (%)	Δ_P (mm)	F_u (kN)	Δ_u (mm)
RS	11.92	–	1.37	18.22	–	9.99	15.47	16.17
SY-C0	17.70	48	1.93	22.19	22	18.02	18.86	20.90
SN-C1	15.23	28	1.82	29.03	59	20.89	24.00	23.60
SY-C1	20.28	70	2.15	31.70	74	20.31	26.94	22.13
SY-C2	23.80	100	2.34	39.96	119	26.37	31.44	28.41
SY-C3	25.34	113	2.68	42.26	132	33.10	34.29	36.25

from carbon fibers coated with epoxy on the surface. In the process of the test, the outermost fibers filament reached the ultimate tensile strength first and then ruptured due to the great bonding property between the outermost fibers and the matrix. Therefore, the core fibers filaments were separated from the outermost fibers filament, resulting in them not being able to afford the tensile force together. The tensile strength of the textile was not fully utilized. It could also be seen that the peak deflection of strengthened specimens was greatly improved. The justification was the ultimate tensile strain of TRHDC composites enhanced with the increase of the textile layers, as shown in Table 4. Thus, the strengthening layer with the multilayer textile could still work under a large slab deflection.

3.3 Serviceability limit state analysis

In practical engineering, the slabs may be out of work due to wide cracks or excessive deflection. The code [25] stipulated that the slabs met their serviceability limit state when the slabs deflection reached 1/200 of the span distance. The load (F_s) and deflection (Δ_s) at the

Table 6 Test results at serviceability limit state

Specimen	F_s (kN)	Increase in F_s (%)	Δ_s (mm)
RS	18.22	–	9.99
SY-C0	20.77	14	12.00
SN-C1	24.05	31	12.11
SY-C1	27.62	52	12.00
SY-C2	30.99	70	12.00
SY-C3	33.00	81	12.00

serviceability limit state was listed in Table 6. It could be observed that the reference slabs failed without reaching their serviceability limit state. After being strengthened by TRHDC composites, the slabs performance obtained an obvious improvement. For the specimen SY-C0 only strengthened by HDC, the load at the serviceability limit state was increased by 14%. The increment was moderate as the tensile strength of HDC was low. While for specimens SN-C1, SY-C1, SY-C2, and SY-C3, which equipped the carbon textile in the strengthening layer, the load was increased by 31%, 52%, 70%, and 81%, respectively. The

increment was considerable as the carbon textile owned a high tensile strength.

This study on flexural strengthening focused on non-preload slabs. In practical engineering, the service load existed on the slabs. This service load was very difficult to be unloaded completely before strengthening. Based on the plane section assumption, Table 7 calculated the textile utilization ratio at the serviceability limit state, which considered the different levels of service load on the slabs before being strengthened by TRHDC composites. It could be observed that the textile utilization ratio decreased as the service load level increased, meaning a reduced strengthening efficiency. This can be explained by the strain lags behavior of the strengthening overlay. Specifically, the strain of concrete and longitudinal steel bars owned a value before being strengthened by the TRHDC layer due to the existence of service load. While the tensile strain of the strengthening layer was zero at this moment. When the slab was loaded to the serviceability limit state, the tensile strain of the strengthening layer was less than that of the slabs without service load. Therefore, the strengthening efficiency would be reduced. The slabs should be unloaded as much as possible before strengthening in practical projects.
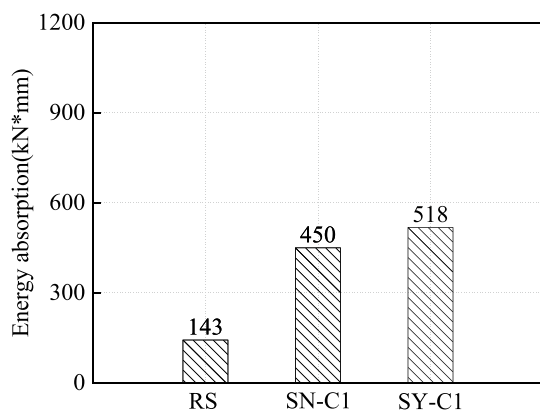
3.4 Energy absorption

In this study, the tensile stress–strain curve of the longitudinal steel bar was shown in Fig. 2. Obviously, the longitudinal steel bar owned no yield platform in the tensile test. The traditional ductility theory which was defined as the ultimate deflection divided by the yield one was not applicable for this study. An energy-based theory was adopted to evaluate the ductility of precast hollow-core slabs in this section. It was calculated by the area under the load–deflection curves before the peak point. The specific value of energy absorption was shown in Fig. 9.
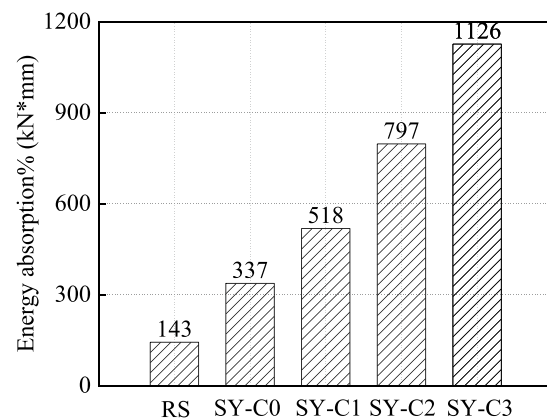
As shown in Fig. 9a, the energy absorption of SY-C1 was higher than that of SN-C1. It indicated that the multiple cracks behavior in the strengthening overlay was conducive to absorbing the energy, which was related to the pulling off or pulling out of PVA fibers. Figure 9b showed that the energy absorption of the strengthened specimens increased greatly as the textile reinforcement ratio increased. In addition to the energy absorption caused by pulling off and pulling out of PVA fibers, another main reason was the carbon textiles stored the work done by the external loads. The textile owned a high tensile strength. In the process of testing, the textiles played the role of longitudinal steel bars to afford the tensile force, as well as absorb the energy.

Table 7 Textile utilization ratio considering the service load level

Textile layers	Textile utilization ratio (%)									
	$0.0\,F_p$	$0.1\,F_p$	$0.2\,F_p$	$0.3\,F_p$	$0.4\,F_p$	$0.5\,F_p$	$0.6\,F_p$	$0.7\,F_p$	$0.8\,F_p$	$0.9\,F_p$
One layer	13.67	12.44	11.21	9.97	8.73	7.50	6.26	5.03	3.80	2.56
Two layer	13.45	12.24	11.03	9.81	8.61	7.39	6.18	4.97	3.77	2.56
Three layer	13.24	12.05	10.86	9.68	8.48	7.30	6.10	4.92	3.74	2.56

(a) Effect of HDC added with or without PVA fibers

(b) Effect of textile reinforcement ratio

Fig. 9 Energy absorption

3.5 Strain analysis

The concrete strain distribution along the height of specimen SY-C1 was shown in Fig. 10. The specific measuring point of concrete strain gauges was introduced in Sect. 2.4. Before cracking, the concrete strain increased slowly as the whole section worked together to afford the external load. After cracking, the increasing ratio of concrete strain was accelerated. And the neutral axis of specimen SY-C1 moved upward slowly, as shown in Fig. 11. Overall, the strain distribution of concrete along the height was approximately linear during the test process, satisfying the assumption of plane section. And no apparent slippage was observed between the strengthening overlay and concrete substrate in all specimens, indicating that the TRHDC composites could cooperate well with the initial slabs to resist the external load.

4 Calculation method in characteristic points

4.1 Basic assumptions

From the strain analysis in Sect. 3.5, the concrete strain distribution along the specimen height was approximately linear. Therefore, to simplify the calculation, it was assumed that:

(i) The plane sections remained planes during the test process;
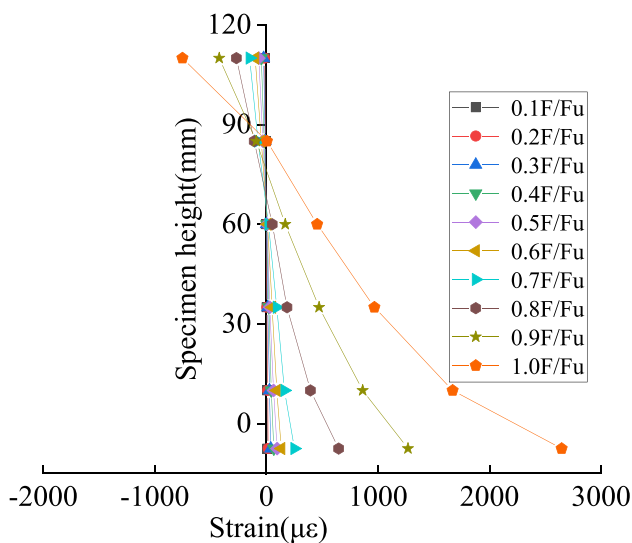(ii) The tensile stress provided by the concrete in the tension zone was ignored after cracking;

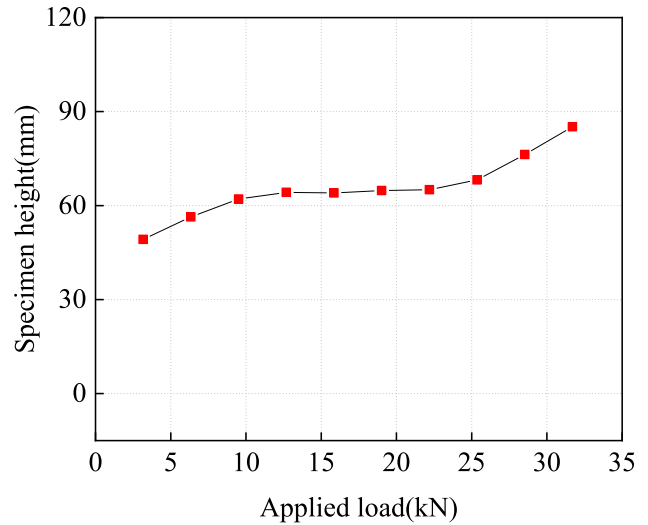**Fig. 10** Concrete strain distribution along the height of specimen SY-C1

Fig. 11 Location of the neutral axis

(iii) The specimens were failed when the longitudinal steel bars fractured or the textiles ruptured;
(iv) Based on the equality of the area and the moment of inertia, the cross-section of the specimens was equivalent to that shown in Fig. 12.

4.2 Constitutive models

4.2.1 Concrete

The precast hollow-core slabs were cast by normal concrete. The compressive constitutive model of normal concrete was recommended by GB 50010-2010 [25], which consisted of a quadratic parabola and a horizontal line. The specific formulas were as follows:

$$\sigma_c = \begin{cases} f_c \left[2\dfrac{\varepsilon_c}{\varepsilon_0} - (\dfrac{\varepsilon_c}{\varepsilon_0})^2 \right] 0 \leq \varepsilon_c \leq \varepsilon_0 \\ f_c \ \varepsilon_0 < \varepsilon_c \leq \varepsilon_{cu} \end{cases}. \tag{1}$$

The tensile constitutive model of normal concrete was a straight line before cracking. And the value was zero after cracking. It could be expressed as:
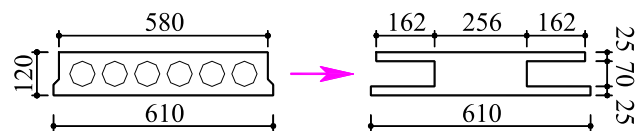

Fig. 12 Diagram of cross-section equivalent

$$\sigma_t = \begin{cases} \dfrac{\varepsilon_t}{\varepsilon_{t0}} f_t & 0 \le \varepsilon_t \le \varepsilon_{t0} \\ 0 & \varepsilon_{t0} < \varepsilon_t \end{cases}, \tag{2}$$

where ε_c and σ_c were the compressive strain and strength of concrete at any point; ε_0 and ε_{cu} were the peak and ultimate compressive strain of concrete; f_c was the uniaxial compressive strength of concrete; ε_t and σ_t were the tensile strain and strength of concrete at any point; ε_{t0} and f_t were the peak tensile strain and strength of concrete.

4.2.2 Longitudinal steel bars

The tensile constitutive model of longitudinal steel bars, which owned no obvious yield platform, was provided by GB 50010-2010 [25]. It could be given by:

$$\sigma_s = \begin{cases} E_s \varepsilon_s & 0 \le \varepsilon_s \le \varepsilon_{y,r} \\ f_{y,r} + k(\varepsilon_s - \varepsilon_{y,r}) & \varepsilon_{y,r} < \varepsilon_s < \varepsilon_u \\ 0 & \varepsilon_s > \varepsilon_u \end{cases}, \tag{3}$$

where ε_s and σ_s were the tensile strain and strength of longitudinal steel bars at any point; E_s was the elastic modulus of the longitudinal steel bars; $f_{y,r}$ was the yield load of longitudinal steel bars, and it was taken as 80% of the ultimate tensile stress; $\varepsilon_{y,r}$ and ε_u were the yield and ultimate tensile strain of longitudinal steel bars.

4.2.3 TRHDC composites

Dong et al. [16, 22] investigated the uniaxial tensile properties of TRHDC composites systematically. Based on the experimental results, the investigation proposed a constitutive model of TRHDC composites, which considered the effect of PVA fibers. In this study, the tensile behaviors of TRHDC samples were similar to that in Refs. [16, 22]. Therefore, the constitutive model of TRHDC composites as Dong et al. suggested was adopted in this study:

$$\sigma_{fe} = \begin{cases} \dfrac{\varepsilon_{fe}}{\varepsilon_{fe,cr}} \sigma_{fe,cr} & (0 \le \varepsilon_{fe} \le \varepsilon_{fe,cr}) \\ \left(\sigma_{cr} - \dfrac{\sigma_{fe,u} - \sigma_{fe,cr}}{\varepsilon_{fe,u} - \varepsilon_{fe,cr}} \varepsilon_{cr}\right) + \dfrac{\sigma_{fe,u} - \sigma_{fe,cr}}{\varepsilon_{fe,u} - \varepsilon_{fe,cr}} \varepsilon_{fe} & (\varepsilon_{fe,cr} < \varepsilon_{fe} \le \varepsilon_{fe,u}) \end{cases}, \tag{4}$$

where ε_{fe} and σ_{fe} were the tensile strain and strength of TRHDC composites at any point; $\varepsilon_{fe,cr}$ and $\sigma_{fe,cr}$ were the cracking strain and strength of TRHDC composites; $\varepsilon_{fe,u}$ and $\sigma_{fe,u}$ were the peak strain and strength of TRHDC composites.

4.3 Determination of failure modes

As the textile reinforcement ratio increased, the compressive concrete strain at the edge of the compression zone was also increased. Once the amount of textile was abundant, the concrete strain would reach its ultimate compressive strain, meaning the concrete was crushed. In general, the precast hollow-core slabs strengthened by TRHDC composites may suffer the following two failure modes. (i) Tensile failure mode: with a low textile reinforcement ratio, the textile ruptured at failure, while the concrete strain at the edge of the compression zone had not reached at its ultimate compressive strain. (ii) Compressive failure mode: with a high textile reinforcement ratio, the concrete strain at the edge of the compression zone reached at its ultimate compressive strain and failed. At this moment, the textile was not ruptured.

In this study, $\rho_{fe,min}$ was used as a theoretical basis for the judgment of the failure mode. $\rho_{fe,min}$ stood for the boundary failure of (i) and (ii). It could be calculated by the simultaneous occurrence of the ultimate compressive strain of concrete and peak tensile strain of strengthening overlay. Once the textile reinforcement ratio ρ_{fe} was calculated as $\rho_{fe} \le \rho_{fe,min}$ or $\rho_{fe} \ge \rho_{fe,min}$, the failure mode of (i) or (ii) would be observed, respectively. Based on assumptions in Sect. 4.1, the stress and strain distribution of specimens was shown in Fig. 13. According to the strain geometric relationship in Fig. 13, the strain relationship in the boundary failure could be obtained as follow:

$$\frac{\varepsilon_{cu}}{h_1} = \frac{\varepsilon_{fe,u}}{h_{fe} - h_1}. \tag{5}$$

Based on the strain compatibility and force equilibrium, the theoretical calculation formula $\rho_{fe,min}$ could be deduced:

$$\rho_{fe,min} = \frac{A_{fe}}{bt} = \frac{f_c b \varepsilon_{cu} h_{fe}}{bt(\varepsilon_{cu} + \varepsilon_{fe,u})\sigma_{fe,u}} - \frac{\sigma_s A_s}{bt\sigma_{fe,u}}. \tag{6}$$
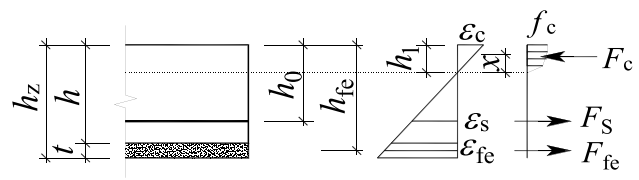

Fig. 13 Stress and strain distribution of cross-section

4.4 Calculation of flexural capacity in characteristic points

4.4.1 Cracking load

The cracking load was obtained by the strain of concrete or TRHDC composites in the tensile side reached its cracking strain. Based on the strain compatibility and force equilibrium, the formulas were as follows:

$$\begin{cases} \sum N = 0, k_1 f_c b h_1 - 0.5 f_t \left(\dfrac{\varepsilon_t}{\varepsilon_{t0}} \right) b(h - h_1) - f_y A_s \left(\dfrac{\varepsilon_s}{\varepsilon_y} \right) - \sigma_{fe,cr} A_{fe} \left(\dfrac{\varepsilon_{fe}}{\varepsilon_{fe,cr}} \right) = 0 \\[2mm] \sum M = 0, M_{cr} = k_2 f_c b h_1^2 + \dfrac{1}{3} f_t \left(\dfrac{\varepsilon_t}{\varepsilon_{t0}} \right) b(h - h_1)^2 + f_y A_s \left(\dfrac{\varepsilon_s}{\varepsilon_y} \right)(h_0 - h_1) \\[2mm] + \sigma_{fe,cr} A_{fe} \left(\dfrac{\varepsilon_{fe}}{\varepsilon_{fe,cr}} \right)(h_{fe} - h_1) \end{cases} \tag{7}$$

4.4.2 Peak load

The peak load was calculated by the longitudinal steel bars or TRHDC composites reached at its peak strain. Similarly, the formulas could be expressed as:

$$\begin{cases} \sum N = 0, k_1 f_c b h_1 - [f_{y,r} + k(\varepsilon_s - \varepsilon_{y,r})] A_s - \sigma_{fe,u} A_{fe} = 0 \\[2mm] \sum M = 0, M_u = k_2 f_c b h_1^2 + [f_{y,r} + k(\varepsilon_s - \varepsilon_{y,r})] A_s (h_0 - h_1) + \sigma_{fe,u} A_{fe}(h_{fe} - h_1) \end{cases} \tag{8}$$

where A_s and A_{fe} were the area of the longitudinal steel bars and TRHDC composite; k_1 and k_2 could be calculated by Eq. (9).

$$\begin{cases} k_1 = \dfrac{\varepsilon_c}{\varepsilon_0} - \dfrac{\varepsilon_c^2}{3\varepsilon_0^2} \\[2mm] k_2 = \dfrac{2\varepsilon_c}{3\varepsilon_0} - \dfrac{\varepsilon_c^2}{4\varepsilon_0^2} \end{cases} \tag{9}$$

According to the strain geometric relationship, as shown in Fig. 13, the strain relationship between the compressive zone concrete, tensile zone concrete, longitudinal steel bars, and TRHDC composites in the cracking and peak points

could be obtained, respectively. Then, the stress provided by each part would be derived by substituting the strain into the corresponding constitutive models in Sect. 4.2. Based on the strain compatibility and force equilibrium, the cracking and peak load were calculated by Eqs. (7) and (8), respectively. The calculated values (F_{the}) and experimental values (F_{exp}) in the two points were summarized in Table 8. The ratios of the calculated value divided by the experimental one were also listed in Table 8. The average ratios in the cracking and peak points were 0.94 and 1.05 with the variable coefficient of 0.09 and 0.04, respectively. The calculated values were in good agreement with the experimental values, indicating that the proposed calculation method of flexural capacity owned a theoretical accuracy. It could be the theoretical basis of practical application.

4.5 Simplified calculation method for peak load

From the analysis in Sect. 4.3, the tensile failure, which was caused by the textile rupture, was the most dangerous in the application of TRHDC composites. Therefore, the textile reinforcement ratio ρ_{fe} should be calculated to be greater than the $\rho_{fe,min}$ in practical application, firstly. The purpose was to ensure that ductile compressive failure mode could be observed in practical engineering. In Sect. 2.3.2, the tensile strength of TRHDC composites was obtained by testing the dog-bone-shaped samples. However, it could also be calculated by Eq. (10), which considered the utilization rate of carbon textiles [16, 22].

$$\sigma_{fe,u} = k\rho_f f_{f,u}, \tag{10}$$

where k was the utilization rate of carbon textiles; ρ_f was the textile reinforcement ratio; $f_{f,u}$ was the ultimate tensile strength of carbon textiles.

When TRHDC was used for flexural strengthening of slabs, Eq. (11) for the textile utilization rate was given based on the plane section assumption [29].

$$k = \frac{\beta\varepsilon_{cu} h_f / x - \varepsilon_{cu} - \varepsilon_{f0}}{\varepsilon_f}, \tag{11}$$

Table 8 Calculated and experimental values in characteristic points

Specimen	$F_{cr,the}$(kN)	$F_{cr,exp}$(kN)	$F_{cr,the}/F_{cr,exp}$	$F_{u,the}$(kN)	$F_{u,exp}$(kN)	$F_{u,the}/F_{u,exp}$
RS	11.97	11.92	1.01	19.03	18.22	1.04
SY-C0	15.84	17.70	0.90	24.81	22.19	1.12
SN-C1	16.43	15.23	1.08	29.78	29.03	1.02
SY-C1	18.80	20.28	0.93	32.89	31.70	1.04
SY-C2	20.43	23.80	0.86	40.62	39.96	1.02
SY-C3	21.72	25.34	0.86	46.66	42.26	1.10
Avg. (CoV)			0.94 (0.09)			1.05 (0.04)

where β, which were constant values related to the textile layers, were respectively 0.15, 0.16, and 0.16 for one, two, and three layers of carbon textile; ε_{f0} was the strain value of textile before being strengthened by TRHDC composites due to the existence of service load. It could be calculated by Eq. (12).

$$\varepsilon_{f0} = \frac{M_{k0}}{E_s A_s h_0}. \tag{12}$$

By substituting Eq. (11) into Eq. (8), the textile utilization rate considering the level of service load could be calculated and listed in Table 9.

In practical engineering, the value of the textile utilization ratio should be selected based on the service load level. Then, by substituting the value into Eq. (13) which provided the simplified calculation method for slabs strengthened with TRHDC, the ultimate flexural capacity ($F_{u,sim}$) of specimens could be calculated. The calculated values of specimens SY-C1, SY-C2, SY-C3, and specimens with the same strengthening material in Ref. [15] were listed in Table 10 and shown in Fig. 14. It could be observed that the average ratio of the simplified calculation method values divided by the experimental one was 0.93 with the variable coefficient of 0.08. The simplified calculation method values exhibited good agreement with the experimental results, especially for the specimens SY-C1 and MY-C1. This method could be a reference for practical application.

$$\begin{cases} k_1 f_c b h_1 = f_{y,r} A_s + k f_f A_f \\ k_2 f_c b h_1^2 = f_{y,r} A_s (h_0 - x) + k f_f A_f (h_f - x) \end{cases}, \tag{13}$$

where $k_1 = k_2 = 0.8$ if the concrete at the edge of the compression zone is crushed, and k_1, k_2 could be taken as Eq. (9) if the concrete strain at the edge of the compression zone has not reached at its ultimate compressive strain.

5 Conclusion

This study investigated the effect of the TRHDC matrix added with or without PVA fibers and the number of textile layers on the flexural behaviors of precast hollow-core slabs. Six slabs, including one reference slab and five strengthened slabs, were designed and tested as simply supported under four-point bending. The main conclusions were summarized as:

(1) The reference slab failed due to the fracture of longitudinal steel bar. After being strengthened by TRHDC composites, the textile rupture was observed in the five strengthened slabs. The cracking and peak load were greatly enhanced compared to that of the reference slab. While the enhancement ratio provided by carbon textiles was disparate at different stages.

(2) With the addition of PVA fibers in the HDC matrix, the crack width of TRHDC composites could be limited effectively. Obvious multi-crack behavior was observed in the strengthening overlay. Moreover, no apparent slippage was observed between the strengthening overlay and concrete substrate in all specimens, indicating that the TRHDC composites could cooperate well with the initial slabs to resist the external load.

(3) With the increase of textile layers, the mid-span deflection of the strengthened slabs was improved greatly, accompanied by a higher energy absorption capacity compared with the reference slab.

(4) Based on the plane section assumption, a calculation method was proposed to calculate the flexural capacity of slabs strengthened with TRHDC composites. The calculated values were in good agreement with the test values. It could provide a theoretical reference for practical application.

Table 10 Flexural capacity of simplified calculation method values and experimental results

Specimen	$F_{u,sim}$(kN)	$F_{u,exp}$(kN)	$F_{u,sim}/F_{u,exp}$
This manuscript			
SY-C1	31.21	31.70	0.98
SY-C2	37.29	39.96	0.93
SY-C3	40.46	42.26	0.96
Ref. [15]			
MY-C1	41.93	41.41	1.01
MY-C2	48.65	53.13	0.92
MY-C3	52.17	66.03	0.80
Avg. (CoV)			0.93 (0.08)

Table 9 Textile utilization ratio considering the service load level

Textile layers	Textile utilization ratio (%)									
	$0.0\,F_p$	$0.1\,F_p$	$0.2\,F_p$	$0.3\,F_p$	$0.4\,F_p$	$0.5\,F_p$	$0.6\,F_p$	$0.7\,F_p$	$0.8\,F_p$	$0.9\,F_p$
One layer	33.15	30.55	27.98	25.42	22.88	20.37	17.88	15.42	12.97	10.55
Two layer	26.86	24.55	22.28	20.05	17.85	15.69	13.57	11.48	9.42	7.41
Three layer	21.52	19.34	17.21	15.12	13.08	11.08	9.13	7.22	5.35	3.52
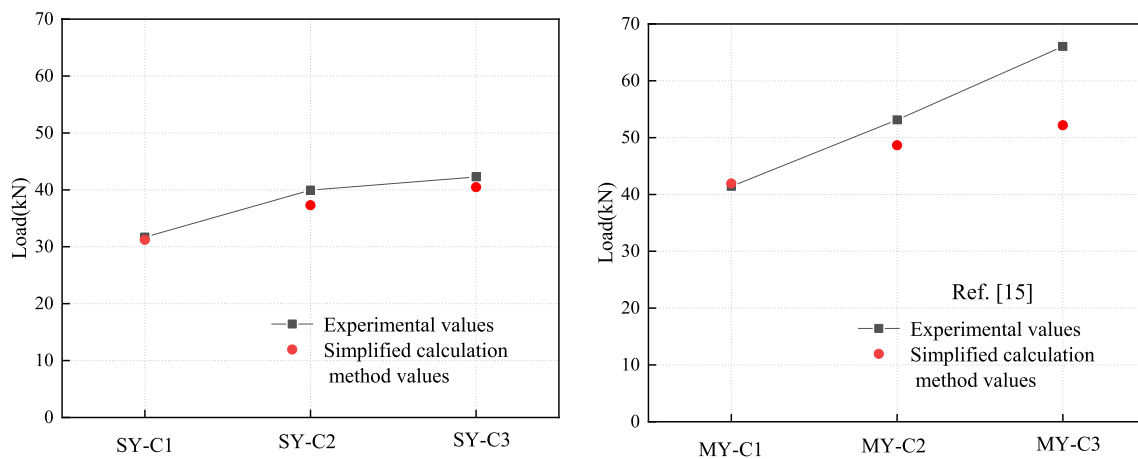
Fig. 14 Comparison of flexural capacity

Author contributions All persons who meet authorship criteria are listed as authors, and all authors certify that they have participated sufficiently in the work to take public responsibility for the content, including participation in the concept, design, analysis, writing, or revision of the manuscript. Conceptualization: SS, MD; Methodology: SS, MD; Validation: SS; Formal analysis: SS; Investigation: SS; Resources: SS, MD; Writing—original draft: SS; Writing—review and editing: SS, MD, JY, RL, YZ; Supervision: MD, YZ; Project administration: SS, MD, JY, RL, YZ; Funding acquisition: MD.

Data availability All data included in this study are available upon request by contact with the corresponding author.

Declarations

Conflict of interest The authors declare that they have no known competing financial interests or personal relationships that could have appeared to influence the work reported in this paper.

Ethical approval This article does not contain any studies with human participants performed by any of the authors.

Informed consent Informed consent was obtained from all individual participants included in the study.

References

1. Souza RHF, Appleton J. Behaviour of shear-strengthened reinforced concrete beams. J Mater Struct Constr. 1997;30:81–6.
2. Altun F. An experimental study of the jacketed reinforced-concrete beams under bending. J Constr Build Mater. 2004;18:611–8.
3. Cheong HK, MacAlevey N. Experimental behavior of jacketed reinforced concrete beams. J Struct Eng. 2000;126:692–9.
4. Fédération internationale du béton. Seismic assessment and retrofit of reinforced concrete buildings: state-of-art report. Int Feder Struct Concrete 2003.
5. Giese ACH, Giese DN, Dutra VFP, Da Silva Filho LCP. Flexural behavior of reinforced concrete beams strengthened with textile reinforced mortar [J]. J Build Eng. 2021;33:2352–7102.
6. Bösche A, Jesse F, Ortlepp R, Weiland S, Curbach M. Textile-reinforced concrete for flexural strengthening of RC structures—Part 1: structural behavior and design model. ACI Spec Publ. 2008;251:19–40.
7. Awani O, El-Maaddawy T, Ismail N. Fabric-reinforced cementitious matrix: a promising strengthening technique for concrete structures. Constr Build Mater. 2017;132:94–111.
8. Koutas LN, Tetta Z, Bournas DA, Triantafillou TC. Strengthening of concrete structures with textile reinforced mortars: state-of-the-art review. J Compos Constr. 2019;23(1):03118001.
9. Gonzalez-Libreros JH, Sabau C, Sneed LH, Pellegrino C, Sas G. State of research on shear strengthening of RC beams with FRCM composites. Constr Build Mater. 2017;149:444–58.
10. Azam R, Soudki K, West JS, Noel M. Strengthening of shear-critical RC beams: alternatives to externally bonded CFRP sheets. Constr Build Mater. 2017;151:494–503.
11. Li VC. On engineered cementitious composites (ECC): a review of the material and its applications. Trans Res Record J Transport Res Board. 2011;2164(1):1–8.
12. Kanda T, Li VC. Practical design criteria for saturated pseudo strain hardening behavior in ECC. J Adv Concr Technol. 2006;4(1):59–72.
13. Li VC, Wang S, Wu C. Tensile strain-hardening behavior of PVA-ECC; 2001.
14. Yang JM, Min KH, Shin HO, Yoon YS. Effect of steel and synthetic fibers on flexural behavior of high-strength concrete beams reinforced with FRP bars. J Compos PartB Eng. 2012;43:1077–86.
15. Dong Z, Deng M, Dai J, Song S. Flexural strengthening of RC slabs using textile reinforced mortar improved with short PVA fibers [J]. Constr Build Mater. 2021;304:0950–1618.
16. Dong Z, Deng M, Zhang C, Zhang Y, Sun H. Tensile behavior of glass textile reinforced mortar (TRM) added with short PVA fibers [J]. Constr Build Mater. 2020;260:0950–0618.
17. Caggegi C, Carozzi FG, De Santis S, Fabbrocino F, Focacci F, et al. Experimental analysis on tensile and bond properties of PBO and aramid fabric reinforced cementitious matrix for strengthening masonry structures. Compos Part B. 2017;127:175–95.

18. Caggegi C, Lanoye E, Djama K, et al. Tensile behavior of a basalt TRM strengthening system: influence of mortar and reinforcing textile ratios. Compos BEng. 2017;130:90–102.
19. Carozzi FG, Bellini A, D'Antino T, De Felice G, Focacci F, et al. Experimental investigation of tensile and bond properties of Carbon-FRCM composites for strengthening masonry elements. Compos Part B. 2017;128:100–19.
20. Leone M, Aiello MA, Balsamo A, Carozzi FG, Ceroni F, et al. Glass fabric reinforced cementitious matrix: tensile properties and bond performance on masonry substrate. Compos Part B. 2017;127:196–214.
21. D'Antino T, Carloni C, Sneed LH, Pellegrino C. Matrix-fiber bond behavior in PBO FRCM composites: a fracture mechanics approach. Eng Fract Mech. 2014;117:94–111.
22. Deng M, Dong Z, Zhang C. Experimental investigation on tensile behavior of carbon textile reinforced mortar (TRM) added with short polyvinyl alcohol (PVA) fibers [J]. Constr Build Mater. 2020;235:0950–0618.
23. Barhum R, Mechtcherine V. Influence of short dispersed and short integral glass fibres on the mechanical behaviour of textile-reinforced concrete. Mater Struct. 2013;46:557–72.
24. CB/T 14040-2007, Code for design of prestressed concrete hollow-core slabs. Beijing: Chinese standard press; 2007.
25. GB50010-2010, Code for design of concrete structures. Beijing: Chinese standard press; 2010.
26. GB/T 2975-2018, Steel and steel products-location and preparation of samples and test pieces for mechanical testing. Beijing: Chinese standard press; 2018.
27. GB.T 36262-2018, Fiber reinforced polymer composite grids for civil engineering. Chinese standard press; 2018.
28. DBJ61/T112–2016, Technical specification for application of high ductile concrete, Xi'an, China; 2016.
29. GB 50367-2013, Code for design of strengthening concrete structures. Beijing: Chinese standard press; 2013.